PRECIPITATION VARIABILITY IN SOUTH AMERICA FROM IPCC-AR4 MODELS
PART II: INFLUENCE OF SH CIRCULATION LEADING PATTERNS

Carolina Vera *, Gabriel Silvestri *, Brant Liebmann [#], Paula Gonzalez *

* CIMA-DCAO, University of Buenos Aires-CONICET, Buenos Aires, Argentina.

[#] NOAA/CIRES, Climate Diagnostics Center, Boulder, Colorado, USA.

1. Introduction

It is well known that the large-scale circulation in the Southern Hemisphere (SH) is dominated by three main leading patterns (Kidson 1988). The Southern Annular Mode (SAM) explains the largest variance percentage and it is characterized by a zonally-symmetric anomaly center located over the Antarctica with opposite phase with those anomalies at middle latitudes (Thompson and Wallace 2000). Kidson and Watterson (1999) and Limpasuvan and Hartmann (2000) suggest that this mode arise from the internal dynamics of the atmosphere. Rossby wavetrains extending from the tropics into the SH extratropics, characterize the spatial distribution of the next two leading modes, usually known as Pacific South American (PSA) patterns. PSA1 emanates from central Pacific equatorial region and extends to South America along an arch path. PSA1 exhibits the largest correlation with El Niño-Southern Oscillation (ENSO). On the other hand, PSA2 emanates from the western tropical Pacific, with anomalies extended from Australia to South America (Mo 2000).

Precipitation over South America exhibits considerable variability on interannual and longer timescales. Among different forcings, the large-scale influence over such variability has been recognized (Vera et al. 2006 and references therein). Grimm et al. (2000) showed that ENSO signal on precipitation anomalies in South America is associated with anomalies in the regional circulation linked to the PSA patterns. SAM also seems to have a significant influence onto the precipitation variability in South America mainly concentrated over the southeastern region and during austral spring (Silvestri and Vera 2003).

How the leading patterns of circulation variability in the SH and their influence onto precipitation variability in South America will change under climate change scenario are key questions. However, in order to address them it is essential to first assess whether the observed modes of variability are reasonably simulated by climate GCMs. Recently, climate modeling groups around the world have been charged in performing an unprecedented set of coordinated 20th and 21st century climate change experiments, for the IPCC Fourth Assessment Report (AR4). Therefore, the objective of this work is to investigate the ability of the IPCC-AR4 climate models in reproducing the main features of the leading modes of variability of the SH circulation and their impact on South America precipitation. Assessment of the changes on the activity of such leading modes and their influence on South American climate on climate change simulations will be subject of future works.

2. Data and methodology

Gridded analyses of observed monthly mean precipitation available at the University of Delaware (UDEL) are used

(climate.geog.udel.edu/~climate/). Monthly mean fields of 500-hPa geopotential heights (Z500) and sea surface temperature (SST) from the NCEP-NCAR reanalysis (Kalnay et al. 1996) were used to describe the large-scale conditions.

The simulation runs are a subset of the climate simulations of the 20th century (20c3m) for the IPCC-AR4. A total of 20 runs from 7 different models, CNRM, GFDL-CM2.0, GISS-EH, IPSL-CM4, MIROC-3.2, ECHAM5 (MPI), and MRI2.3.2, were considered (Table 1).

The study concentrates in the period 1970-99. Anomalies were defined removing the seasonal cycle and the long-term trend. The leading patterns of SH circulation were obtained through the analysis of the Empirical Orthogonal Functions (EOFs) for the Z500 anomalies south of 20ºS. Prior to the EOF analysis, a subset of points was extracted at 5° resolution in latitude and a variable resolution in longitude in order to provide a more even density of points and to avoid biasing the analysis toward high-latitude patterns (Kidson 1999). Computations involving the numerical simulations were first performed per individual run and then the results were averaged over all the runs available for each model.

3. Main features of the leading patterns of the circulation in the SH

Figure 1 shows the regression map between the EOF time-series and the Z500 anomalies for NCEP reanalysis and model simulations. The explained variance of the first three leading patterns for NCEP is 14, 10 and 9% respectively. The corresponding percentages of variance explained by model simulations are similar to those observed, excepting for a few number of models that exhibit a larger percentage of variance related with the first leading pattern while less explained variance associated with tropical forcing.

The first leading mode obtained from NCEP (Fig. 1) clearly shows the main characteristics of the SAM, including the 3-wave pattern at middle latitudes. All models outputs resemble the SAM being the main differences between models and observations concentrated at middle latitudes. Certain dispersion among models is evident, particularly regarding the dominant spatial wavenumber at the extratropics. While some models have evidences of a 3-wave pattern (CNRM, GISS, GFDL, MIROC and MPI) a few of them exhibit a 4-wave pattern (IPSL and MRI).

It is recognized that the SAM is due to the atmosphere internal variability (e.g., Limpasuvan and Hartmann 2000), although some relationship with SST variability is observed in NCEP data (Fig. 2) with extreme negative correlation values over the tropical oceans and along the southern oceans. Figure 2 shows that most models exhibit large and positive correlations along the southern oceans (excepting MPI). At the tropics, CNRM, GFDL and MPI are able to reproduce some negative correlation between SST anomalies and the SAM, although MRI exhibit positive correlations and the rest of the models show almost negligible correlations.

The analysis of the next two leading patterns for NCEP shows that the third pattern is the one that exhibits the largest relationship with the equatorial central Pacific (Fig. 2, Table 2), with a PSA1-like pattern linking the circulation anomalies at the central Pacific and those in the South Atlantic (Fig. 1). Considerable differences

are observed between observations and models and among models, regarding the leading pattern associated with ENSO. Figure 2 and Table 2 show that the second leading modes for GISS, MIROC, GFDL, MRI, CNRM and MPI are the patterns more related with ENSO. Nevertheless, large dispersion is observed among the corresponding circulation anomaly patterns. In particular, the second leading mode of both MIROC and GFDL, also exhibits large correlations with the SST anomalies in the three ocean basins, while GISS and IPSL, are the models that show weakest relationship between the surface ocean variability and that of the circulation in the SH. In addition, second leading patterns of several models also show evidences of annular-like structure that could be due to a SAM related signal that is not only projected onto the first leading pattern but also on the second one.

The second leading mode obtained from NCEP is characterized by a wavetrain extended from Australia towards South America, referred in literature as PSA2 (Mo 2000). Figure 2 shows significant correlation between the NCEP PSA2 and SST anomalies in the central-western Pacific and the tropical Atlantic. On the other hand, the identification of the PSA2-like pattern in model simulations is not easy. While there are models like GISS, MIROC, MRI and GFDL, which their corresponding third leading patterns exhibit a PSA2-like structure, the corresponding patterns for MPI, and CNRM exhibit a wave-like structure more zonally oriented along the SH extratropics.

4. Relationship between the leading patterns and precipitation over South America

Figure 3 shows the correlation between precipitation anomalies in South America and the temporal series of the three leading patterns obtained from NCEP and model simulations. For NCEP, Fig. 3 shows almost no observed relationship between SAM and precipitation in South America excepting along the southern Andes. The fact that the analysis is made over the whole year and not discriminated by seasons, might be affecting this result. Silvestri and Vera (2003) show considerable variations from one season to the other, of the influence of SAM onto precipitation interannual variability over southeastern South America. Figure 3 shows that all models exhibit positive correlations between SAM and a band of precipitation along the extratropics associated with the presence of cyclonic anomalies zonally oriented along that band (Fig. 1, left column)

Central column of Figure 3 shows the relationship between the second leading pattern of circulation variability, associated with ENSO, and precipitation anomalies in South America. The NCEP case shows the typical ENSO-like signal with negative values over tropical South America and positive ones over southeastern South America. GFDL, MPI, and MRI are the models that better depict the observed pattern, models like CNRM and IPSL display opposite correlation signs than observed, while MIROC and GISS have almost no signal.

The most distinctive feature of the correlation map between NCEP third leading pattern and UDEL precipitation anomalies are the region of positive values along the southern tip of continent. Correlation maps between ENSO index and precipitation anomalies in South America (not shown) confirm that they are also related with the variability in the equatorial Pacific. The

corresponding maps for the model simulations show that with the exception of IPSL and MIROC, the rest of the models display along the extratropics, positive correlations between the time series of the third leading pattern of circulation variability and precipitation anomalies, being those over the South Pacific located equatorward than those over the continent and the southwestern Atlantic.

4. Conclusions

The analysis of the three leading patterns of the SH circulation variability from observations and model simulations shows that all models are able to reproduce a first leading pattern resembling the SAM. On the other hand, just some of them can reproduce PSA-like structure associated with the second and third leading patterns. The analysis suggests that GFDL, GISS and MPI are the models that reproduce patterns more similar to those observed.

Regarding the observed relationship between ENSO and SH circulation anomalies and precipitation anomalies in South America, it was found that most of the model second leading patterns are significantly correlated with ENSO. Nevertheless, there is considerable dispersion among models regarding the ENSO amplitude and the SH circulation response to ENSO.

It was also found not only for model results but also for NCEP, that both ENSO-related signal and that of SAM were projected onto more than one EOF. This result can be associated with limitations in the EOF technique in separating physical modes and/or sampling errors associated with the length of the period considered.

The relationship between monthly mean precipitation anomalies and the three leading patterns of SH circulation variability show that most of the models reproduced the SAM influence onto precipitation variability at the southern Andes. On the other hand, just a few of them were able to reproduce the observed influence of both PSA1 and PSA2 on South American precipitation variability. The last result can be associated with model deficiencies in reproducing the ENSO cycle and its remote influence on the SH circulation variability.

References

Grimm, A. M., V. R. Barros and M. E. Doyle, 2000: Climate variability in southern South America associated with El Niño and La Niña events. *J. Climate*, **13**, 35-58.

Kalnay, E. and Coauthors, 1996: The NCEP/NCAR 40-year reanalysis project. *Bull. Amer. Meteor. Soc.*, **77**, 437-471.

Kidson, J.W., 1988: Interannual variations in the Southern Hemisphere circulation. *J. Climate*, **1**, 1177-1198.

Kidson, J.W., 1999: Principal modes of Southern Hemisphere low frequency variability obtained from NCEP-NCAR reanalyses. *J. Climate*, **12**, 2808-2830.

Kidson, J. W., and I. G. Watterson, 1999: The structure and predictability of the "high-latitude mode" in the CSIRO9 general circulation model. *J. Atmos. Sci.*, **56**, 3859-3873.

Limpasuvan, V., and D. L. Hartmann, 2000: Wave-maintained annular modes of climate variability. *J. Climate*, **13**, 4414-4429.

Mo, K. C., 2000: Relationships between low-frequency variability in the Southern Hemisphere and sea surface temperature anomalies. *J. Climate*, **13**, 3599-3620.

Silvestri, G. E., and C. S. Vera, 2003: Antarctic Oscillation signal on precipitation anomalies over southeastern South America. Geophys. Res. Lett., 30(21), doi:10.1029/2003GL018277.

Thompson, D. W. J., and J. M. Wallace, Annular modes in the extratropical circulation. Part I: month-to-month variability. *J. Climate*, **13**, 1000-1016, 2000.

Vera C., W. Higgins, J. Amador, T. Ambrizzi, R. Garreaud, D. Gochis, d. Gutzler, D. Lettenmaier, J. Marengo, C. Mechoso, J. Nogues-Paegle, P. Silva Dias, and C. Zhang, 2006: A Unified View of the American Monsoon Systems, *J. Climate*. In press.

Figure 1: Regression between the EOF time-series and the Z500 anomalies for NCEP reanalysis and model simulations. Positive (negative) values in red (blue).

Figure 2: Correlation between the EOF time-series and the SST anomalies for NCEP reanalysis and model simulations. Positive (negative) values in red (blue). Black lines indicate areas where values are statistically significant at the 95% of a T-Student test.
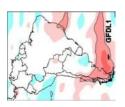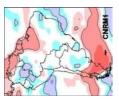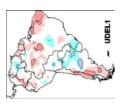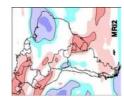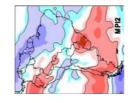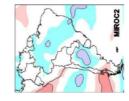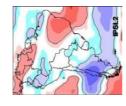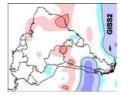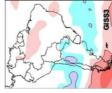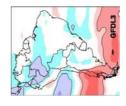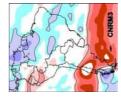
Figure 3: As Fig.2 but for precipitation.
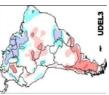
Acronym	Model Name	N° of Runs	*Resolution*
OBS	NCEP Reanalysis CMAP precipitation	-	2.5°x2.5°
CNRM	Meteo France CNRM	1	2.8°x2.8°
GFDL	NOAA Geophysical Fluid Dynamics Laboratory, CM2.0	3	2.5°x2.
GISS	NASA/GODDARD Institute for Space Studies, ModelE20/HYCOM	5	5°x4°
IPSL	Institute Pierre Simon Laplace CM4	1	3.75°x2.5°
MIROC	CSSR/NIES/FRGC, JAPAN, MIROC3.2 Medium resolution	3	2.8°x2.8°
MPI	Max Planck Institute –ECHAM5	2	1.875°x1.875°
MRI	Meteorological Research Institute Japan, CGM2.3.2a	5	2.8°x2.8°
	Total Number of simulations	**20**	

Table 1: List of climate simulations considered.

MODEL	EOF 1	EOF 2	EOF 3
NCEP	**-0.22**	**0.26**	**0.53**
CNRM	-0.06	**0.51**	**0.28**
GFDL	**-0.12**	**0.41**	**0.29**
GISS	**-0.11**	0.08	0.02
IPSL	**-0.21**	**0.15**	**0.14**
MIROC	**-0.28**	**0.43**	0.06
MPI	**-0.11**	**0.58**	**0.24**
MRI	0.09	**0.43**	0.03

Table 2: Correlation between the EOF time-series and the SST anomalies in EN3.4 region. Values statistically significant at the 95% of a T-Student test are in red.